Open Access Article

Ann. Acad. Med. Siles. (Online) 2026;80:274–290
eISSN 1734-025X
DOI: 10.18794/aams/222524
www.annales.sum.edu.pl

PRACA ORYGINALNA
ORIGINAL PAPER

Dose-dependent effects of Er:YAG laser on human fibroblast proliferation, cell death, and γH2AX DNA damage signaling

Wpływ lasera Er:YAG na proliferację ludzkich fibroblastów, śmierć komórkową oraz sygnalizację uszkodzeń DNA z udziałem γH2AX

Jakub Fiegler-Rudol[1], Jacek Matys[2], Robert D. Wojtyczka[3], Dariusz R. Skaba[4], Rafał Wiench[4]

[1]PhD Candidate, Department of Periodontal Diseases and Oral Mucosa Diseases, Faculty of Medical Sciences in Zabrze, Medical University of Silesia, Katowice, Poland

[2]Department of Dental Surgery, Wroclaw Medical University, Poland

[3]Department of Microbiology, Faculty of Pharmaceutical Sciences in Sosnowiec, Medical University of Silesia, Katowice, Poland

[4]Department of Periodontal Diseases and Oral Mucosa Diseases, Faculty of Medical Sciences in Zabrze, Medical University of Silesia, Katowice, Poland

ABSTRACT

INTRODUCTION: The biological response of fibroblasts to Er:YAG laser irradiation is dose-dependent, yet the threshold between biologically tolerable and cytotoxic exposure remains insufficiently defined. The aim of the study is to evaluate dose-dependent effects of Er:YAG laser irradiation (80–180 mJ) on proliferation, apoptosis/necrosis, and γH2AX--associated DNA damage signaling in human fibroblasts in vitro.

MATERIAL AND METHODS: Human foreskin fibroblasts (HFF-1) were exposed to Er:YAG irradiation (2940 nm; 10 Hz; 300 µs; 3 min) at 80, 130, or 180 mJ and compared with mock-treated controls. Proliferation was assessed by 24 h time-lapse fluorescence imaging. Apoptosis and necrosis were quantified by Annexin V/EthD-III staining, and DNA damage by immunofluorescent γH2AX detection. Three independent biological replicates were performed; ANOVA with post hoc testing was applied ($p < 0.05$).

RESULTS: Irradiation induced dose-dependent proliferation suppression, significant in the 180 mJ group from 10 h onward and in all irradiated groups from 14 h ($p \leq 0.03$), with increasing magnitude at higher energies ($p < 0.001$). Apoptosis and necrosis were unaffected at 80 and 130 mJ ($p > 0.05$), whereas 180 mJ produced marked increases in both ($p < 0.001$). γH2AX signal remained unchanged at lower energies but was significantly elevated at 180 mJ ($p < 0.001$).

CONCLUSIONS: A biological transition appears to occur between 130 and 180 mJ, characterized by proliferative arrest, activation of cell death pathways, and increased γH2AX-associated DNA damage signaling. These findings are indicative rather than definitive and require validation in refined experimental models prior to clinical translation.

KEYWORDS

Er:YAG laser, fibroblasts, γH2AX, apoptosis, necrosis, proliferation, dose–response, laser safety

Received: 18.05.2026 **Revised:** 21.05.2026 **Accepted:** 27.05.2026 **Published online:** 16.06.2026

Address for correspondence: Jakub Fiegler-Rudol, Katedra i Zakład Chorób Przyzębia i Błony Śluzowej Jamy Ustnej, Wydział Nauk Medycznych w Zabrzu ŚUM, pl. Traugutta 2, 41-800 Zabrze, tel. +48 32 271 36 12, e-mail: jakub.fieglerrudol@gmail.com

Publisher: Medical University of Silesia, Katowice, Poland

STRESZCZENIE

WSTĘP: Odpowiedź biologiczna fibroblastów na naświetlanie laserem Er:YAG jest zależna od dawki, jednak próg między ekspozycją biologicznie tolerowaną a cytotoksyczną pozostaje niedostatecznie określony. Celem badania jest ocena zależnych od dawki efektów naświetlania laserem Er:YAG (80–180 mJ) na proliferację, apoptozę/nekrozę oraz sygnalizację uszkodzeń DNA związaną z γH2AX w ludzkich fibroblastach w warunkach in vitro.
MATERIAŁ I METODY: Ludzkie fibroblasty napletka (*human foreskin fibroblasts* – HFF-1) poddano naświetlaniu laserem Er:YAG (2940 nm; 10 Hz; 300 µs; 3 min) przy energiach 80, 130 lub 180 mJ i porównano z grupą kontrolną, poddaną procedurze pozorowanej. Proliferację oceniano za pomocą 24-godzinnego mikroskopowego obrazowania poklatkowego z fluorescencją. Apoptozę i nekrozę oznaczano barwieniem Aneksyną V/EthD-III, a uszkodzenia DNA za pomocą immunofluorescencyjnego wykrywania γH2AX. Przeprowadzono trzy niezależne repliki biologiczne; zastosowano analizę ANOVA z testami post hoc ($p < 0,05$).
WYNIKI: Naświetlanie indukowało zależne od dawki zahamowanie proliferacji, istotne w grupie 180 mJ od 10. godziny, a we wszystkich naświetlanych grupach od 14. godziny ($p \leq 0,03$), nasilające się wraz ze wzrostem energii ($p < 0,001$). Apoptoza i nekroza nie uległy istotnym zmianom przy 80 i 130 mJ ($p > 0,05$), natomiast 180 mJ spowodowało wyraźny wzrost obu parametrów ($p < 0,001$). Ekspresja γH2AX pozostawała niezmieniona przy niższych energiach, lecz była istotnie podwyższona przy 180 mJ ($p < 0,001$).
WNIOSKI: Wyniki wskazują na biologiczny punkt przejścia między 130 a 180 mJ, charakteryzujący się zatrzymaniem proliferacji, aktywacją szlaków śmierci komórkowej oraz nasiloną sygnalizacją uszkodzeń DNA związaną z γH2AX. Uzyskane dane mają charakter wskazujący, a nie definitywny, i wymagają walidacji w udoskonalonych modelach eksperymentalnych przed zastosowaniem klinicznym.

SŁOWA KLUCZOWE

laser Er:YAG, fibroblasty, γH2AX, apoptoza, nekroza, proliferacja, zależność dawka–odpowiedź, bezpieczeństwo laserowe

INTRODUCTION

The erbium-doped yttrium–aluminum–garnet (Er:YAG) laser is widely used in dermatology, periodontics, and regenerative medicine, with applications ranging from ablative skin resurfacing to wound healing [1,2,3]. Operating at 2940 nm, it exhibits high water absorption, enabling precise tissue ablation with minimal collateral thermal damage [4,5]. At subablative energy densities, Er:YAG irradiation can also promote cellular proliferation, migration, and tissue regeneration [6,7,8].

Previous studies have shown that low-level Er:YAG irradiation stimulates fibroblast proliferation via upregulation of galectin-7 and prostaglandin E2 (PGE2) production through cyclooxygenase-2 (COX-2) expression [1,2,5], enhancing the proliferative and migratory capacity of fibroblasts [3,4]. These effects are attributed to photon absorption by mitochondrial cytochrome c oxidase, leading to increased adenosine triphosphate (ATP) production, modulation of reactive oxygen species (ROS), and activation of downstream proliferative signaling [9,10,11].

However, the therapeutic window for Er:YAG laser application remains poorly defined. Higher energy densities can induce cellular stress, DNA damage, and cell death [12,13,14], including vacuolization, hydropic degeneration, epidermal necrosis, and p53-mediated stress responses [14]. Clinical complication rates range from 10% to 38% depending on treatment parameters [15,16,17]. Despite this, systematic dose–response characterization of Er:YAG effects on fibroblast proliferation, apoptosis, necrosis, and DNA damage response has not been performed in controlled in vitro systems. Phosphorylation of histone H2AX (γH2AX) provides a sensitive biomarker of DNA double-strand breaks and genotoxic stress [17]. Concurrent assessment of γH2AX, apoptosis, necrosis, and proliferation enables comprehensive characterization of cellular fate decisions across energy doses, essential for evidence-based protocol optimization in wound healing, tissue remodeling, and regenerative medicine.

This in vitro study aimed to quantitatively characterize the dose-dependent effects of Er:YAG laser irradiation on human fibroblast proliferation dynamics, apoptotic and necrotic cell death, and γH2AX-associated DNA damage signaling, to identify a transition range between biologically tolerated and cytotoxic responses under controlled conditions.

MATERIAL AND METHODS

Study design

This in vitro study evaluated Er:YAG laser effects on human fibroblast proliferation, apoptosis/necrosis, and γH2AX signaling at three energy settings (80 mJ, 130 mJ, 180 mJ) versus non-irradiated controls across three phases:

(I) Time-lapse fluorescence microscopy for morphology and proliferation
(II) Apoptosis/necrosis detection
(III) γH2AX immunofluorescence.

All experiments were performed in three independent biological replicates (N = 3), with 12–15 technical replicates per condition for proliferation and 15 per condition for apoptosis/necrosis and γH2AX analyses.

Cell culture

Human foreskin fibroblasts (HFF-1; ATCC SCRC-1041) were cultured at 37°C, 5% CO_2. Cells at passages 3–8, freshly thawed from cryopreserved stocks, were used. All culture surfaces were pre-coated with 1% Geltrex LDEV-Free Reduced Growth Factor Basement Membrane Matrix (Gibco, Thermo Fisher Scientific, Waltham, MA, USA, Cat. No. 11965092).

Laser irradiation protocol

After 24 h of attachment, fibroblasts were exposed to Er:YAG irradiation at 80, 130, or 180 mJ for 3 minutes. Within this window, 80 mJ was chosen as the lower boundary previously associated with sub-stimulatory to mildly stimulatory effects, 130 mJ as an intermediate value representing approximately the midpoint of the functionally relevant range, and 180 mJ as the upper test dose approaching but not exceeding the energy at which overt cytotoxic effects were anticipated based on preliminary observations [18]. These three levels were thus designed to span a gradient from biologically tolerable to potentially cytotoxic exposure. Irradiation was performed using an AdvErL Evo Er:YAG system (J. Morita, Osaka, Japan; 2940 nm, 10 Hz, 300 µs pulse duration) with a C600F tip (diameter 0.6 mm; area ≈ 0.0028 cm²) in contact mode, in the presence of 100 µL residual culture medium. Applied fluences were 28.6 J/cm² (80 mJ), 46.4 J/cm² (130 mJ), and 64.3 J/cm² (180 mJ). The same tip and geometry were used throughout, ensuring comparable local energy delivery across assay formats. To ensure reproducibility of energy delivery, the tip was repositioned to a standardized central location within each well prior to every irradiation session, using a fixed-mount mechanical holder that maintained a perpendicular orientation and zero airgap throughout contact-mode delivery. Mock-treated controls underwent identical handling without laser activation.

Proliferation assessment (time-lapse imaging)

HFF-1 cells (30,000/well) were seeded onto Geltrex-coated black 24-well glass-bottom plates (ibidi, Cat. No. 82406). Following irradiation, cells were incubated with NucSpot Live 650 Nuclear Stain (Biotium, Cat. No. 40082) for 30 minutes at 37°C. Time-lapse imaging was performed over 24 h on an Olympus IX fluorescence microscope (Lumencor Spectra X, 647 nm; 10-minute intervals). Proliferation ratio was calculated as cell count at each time point (2–24 h) divided by baseline count (0 h), using automated machine learning–assisted nuclear detection in Olympus cellSens software.

Apoptosis and necrosis (Annexin V / EthD-III Assay)

Cells (50,000/well) were seeded onto Geltrex-coated 4-chamber glass-bottom slides (Falcon, Corning). After irradiation, cells were preincubated with NucSpot Nuclear Stain (Biotium, Cat. No. 40081) for 1 hour, then assessed using the Apoptotic, Necrotic and Healthy Cells Quantification Kit (Biotium, Cat. No. 30065) per manufacturer protocol. Cells were incubated with Annexin V and Ethidium Homodimer III (EthD-III) in binding buffer for 15 minutes, washed, and imaged on an Olympus IX microscope at 20× and 40×.

γH2AX immunofluorescence

Cells on Geltrex-coated (1%, LDEV-Free) coverslips were fixed with 4% methanol-free formaldehyde (Thermo Fisher Scientific, Cat. No. 28908), permeabilized with PBS-Triton X, and blocked with 10% normal donkey serum (Sigma-Aldrich, Cat. No. D9663) in 0.1% PBS-Tx. Primary antibody (anti-phospho-H2AX Ser139, clone JBW301, 1:200; EDM Millipore) was applied overnight at 4°C, followed by Alexa Fluor 568 anti-mouse IgG secondary antibody (1:400; Invitrogen, Cat. No. A10037). Nuclei were counterstained with Hoechst (0.5 µg/mL). Coverslips were mounted with Fluorescence Mounting Medium (Dako, Cat. No. S3023). γH2AX-positive cells were defined as nuclei with detectable intranuclear foci above background, expressed as a percentage of total nuclei per field (5 fields per condition, 3 replicates). Negative controls omitted primary antibody. Imaging was performed on an Olympus IX83 at 20× and 40×.

Statistical analysis

Data are presented as mean ± SEM. Statistical analyses were performed in Prism 8.1.0 (GraphPad, San Diego, California, USA). Two-way ANOVA with Dunnett's test was used for proliferation; one-way ANOVA with Dunnett's test for γH2AX; two-way ANOVA with Tukey's test for apoptosis/necrosis. $p < 0.05$ was considered significant.

RESULTS

Effects of Er:YAG laser irradiation on fibroblast proliferation

Temporal proliferation dynamics

Fibroblast proliferation was monitored over 24 h following Er:YAG laser irradiation at 80 mJ, 130 mJ, and 180 mJ, and compared with mock-treated controls ($N = 3$; $n = 12–15$ per group; two-way ANOVA, Dunnett's test). At baseline (0 h), no differences between groups were observed (all $p > 0.99$). During the early phase (2–8 h), all irradiated groups exhibited slightly lower proliferation compared with mock-treated controls, without statistical significance (2 h: $p = 0.32–0.45$; 4 h: $p = 0.18–0.25$; 6 h: $p = 0.05–0.12$; 8 h: $p = 0.06–0.11$). A trend toward significance was

observed at 6 h in the 80 mJ group (p = 0.05). From 10 h onward, divergence between groups became apparent. A significant reduction was first detected in the 180 mJ group at 10 h (mean difference: 0.2172; 95% CI: 0.0269–0.4075; p = 0.02), while 80 mJ and 130 mJ remained non-significant (p = 0.08 and p = 0.17, respectively). This persisted at 12 h for 180 mJ (mean difference: 0.2412; 95% CI: 0.0509–0.4315; p = 0.008).

Dose-dependent effects on proliferation

At 14 h, all irradiated groups showed significant reductions (80 mJ: mean difference: 0.2301, p = 0.01; 130 mJ: 0.2069, p = 0.03; 180 mJ: 0.3018, p < 0.001). From 16 h onward, all irradiated groups remained significant (all p < 0.001), with effect sizes increasing progressively with energy level and over time; full mean-difference values for each time point and energy level are provided in Table I. Mock-treated fibroblasts showed continuous proliferative increase, while all irradiated groups exhibited sustained attenuation with earlier onset and greater magnitude at higher energy levels, particularly 180 mJ (Figure 1; Figures S1–S4 [Figures S1–S6 are included at the end of the article in the Supplementary Materials]).

Table I. Mean differences in proliferation ratio (irradiated vs. mock-treated controls) at 14–24 h. Data presented as mean difference (95% CI); two-way ANOVA with Dunnett's test

Time (h)	Comparison	Mean difference	95% CI	Significant	Symbol	p value
14	untreated vs. 80 mJ	0.2301	0.04316 to 0.4171	Yes	*	0.01
	untreated vs. 130 mJ	0.2069	0.01996 to 0.3939	Yes	*	0.03
	untreated vs. 180 mJ	0.3018	0.1115 to 0.4921	Yes	***	<0.001
16	untreated vs. 80 mJ	0.3081	0.1211 to 0.4950	Yes	***	<0.001
	untreated vs. 130 mJ	0.3056	0.1186 to 0.4926	Yes	***	<0.001
	untreated vs. 180 mJ	0.3864	0.1961 to 0.5767	Yes	***	<0.001
18	untreated vs. 80 mJ	0.3149	0.1280 to 0.5019	Yes	***	<0.001
	untreated vs. 130 mJ	0.3267	0.1397 to 0.5136	Yes	***	<0.001
	untreated vs. 180 mJ	0.4540	0.2637 to 0.6443	Yes	***	<0.001
20	untreated vs. 80 mJ	0.4008	0.2138 to 0.5878	Yes	***	<0.001
	untreated vs. 130 mJ	0.3867	0.1997 to 0.5736	Yes	***	<0.001
	untreated vs. 180 mJ	0.5560	0.3658 to 0.7463	Yes	***	<0.001
22	untreated vs. 80 mJ	0.3845	0.1975 to 0.5714	Yes	***	<0.001
	untreated vs. 130 mJ	0.3708	0.1836 to 0.5578	Yes	***	<0.001
	untreated vs. 180 mJ	0.5474	0.3572 to 0.7377	Yes	***	<0.001
24	untreated vs. 80 mJ	0.5216	0.3052 to 0.7379	Yes	***	<0.001
	untreated vs. 130 mJ	0.4872	0.2708 to 0.7035	Yes	***	<0.001
	untreated vs. 180 mJ	0.7836	0.5605 to 1.007	Yes	***	<0.001

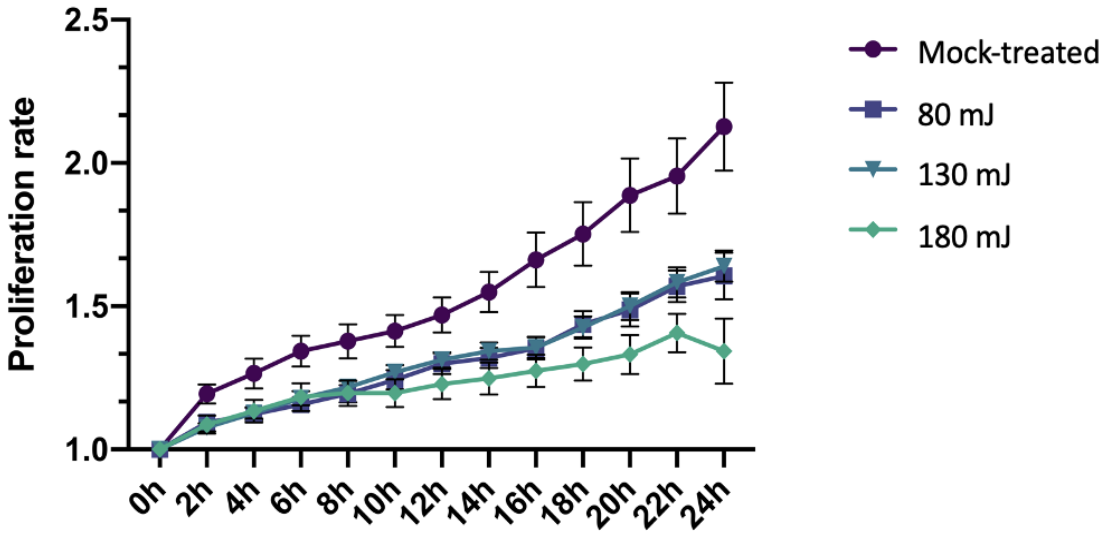

Fig. 1. Effects of Er:YAG laser irradiation on fibroblast proliferation over time

Effects of Er:YAG laser irradiation on apoptosis and necrosis

Annexin V (early apoptosis)

The percentage of Annexin V-positive cells was assessed (N = 3; n = 15; two-way ANOVA, Tukey's test). Mean differences are expressed as untreated minus irradiated, such that negative values indicate higher cell death in the irradiated group. No significant differences were observed between mock-treated controls and the 80 mJ group (mean difference: 0.6260; 95% CI: −0.6440 to 1.896; p = 0.57) or 130 mJ group (mean difference: 0.3327; 95% CI: −0.9373 to 1.603; p = 0.90). The 180 mJ group showed a significantly higher percentage of Annexin V-positive cells than controls (mean difference: −3.157; 95% CI: −4.427 to −1.887; p < 0.001). No difference was found between 80 mJ and 130 mJ (mean difference: −0.2933; 95% CI: −1.563 to 0.9767; p = 0.93), whereas 180 mJ was significantly higher than both 80 mJ (mean difference: −3.783; 95% CI: −5.053 to −2.513; p < 0.001) and 130 mJ (mean difference: −3.489; 95% CI: −4.759 to −2.219; p < 0.001).

EthD-III (necrosis)

No significant differences were observed between controls and 80 mJ (mean difference: −0.0720; 95% CI: −1.342 to 1.198; p > 0.99) or 130 mJ (mean difference: −0.6273; 95% CI: −1.897 to 0.6427; p = 0.57). The 180 mJ group showed a significant increase in necrotic cells versus controls (mean difference: −4.181; 95% CI: −5.451 to −2.911; p < 0.001) and versus both 80 mJ (mean difference: −4.109; 95% CI: −5.379 to −2.839; p < 0.001) and 130 mJ (mean difference: −3.554; 95% CI: −4.824 to −2.284; p < 0.001). No difference was found between 80 mJ and 130 mJ (mean difference: −0.5553; p = 0.67).

Cell death summary

Low- and moderate-energy irradiation (80 and 130 mJ) did not significantly alter apoptotic or necrotic populations. High-energy irradiation (180 mJ) produced marked, significant increases in both Annexin V- and EthD-III-positive cells (Figures 2 and 3; Figures S5 and S6).

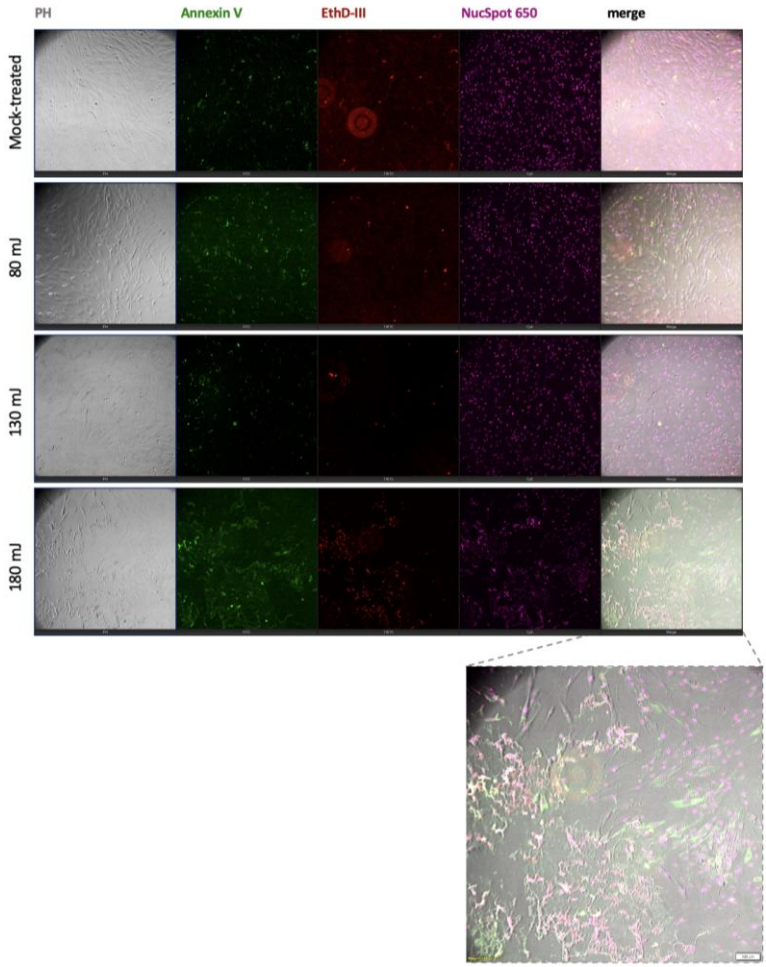

Fig. 2. Annexin V / EthD-III assay. Representative fluorescence and phase contrast images of HFF-1 fibroblasts following Er:YAG laser exposure. Magnification: ×20, lower image enlarged using computer software for better visual presentation

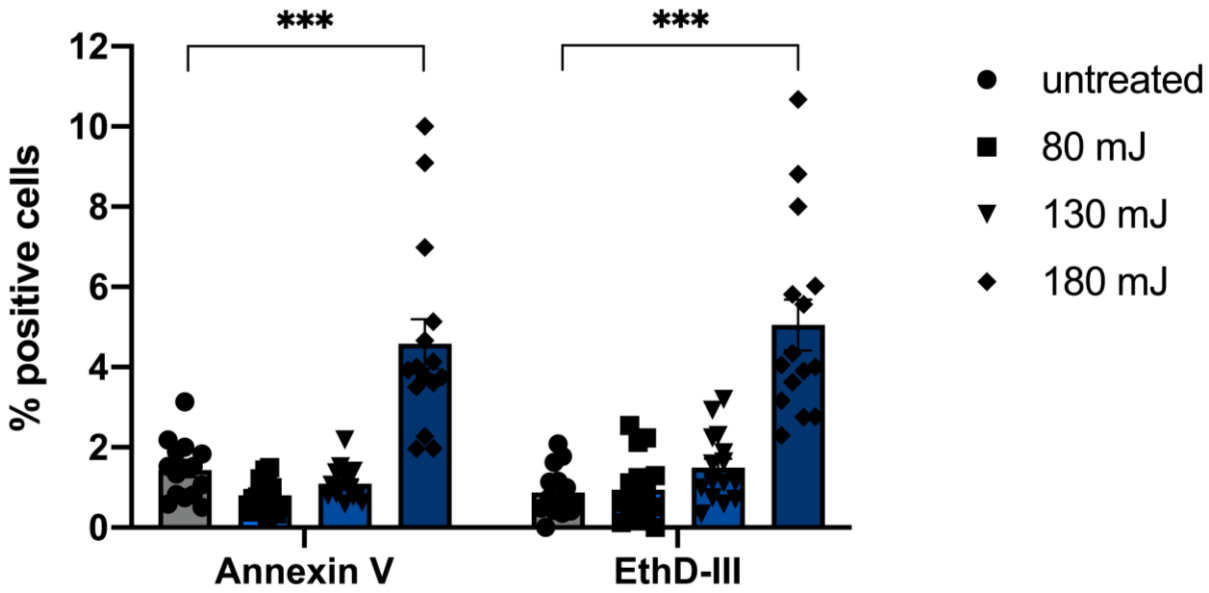

Fig. 3. Effects of Er:YAG laser irradiation on apoptosis and necrosis in human fibroblasts. Quantification of apoptotic (Annexin V-positive) and necrotic (EthD-III-positive) cells following Er:YAG laser irradiation at 80 mJ, 130 mJ, and 180 mJ compared with untreated controls. Data are presented as mean ± SEM (N = 3; n = 15 per group). Statistical analysis: two-way ANOVA, Tukey's test. *** $p < 0.001$

γH2AX-associated DNA damage signaling

γH2AX fluorescence intensity distribution

Qualitative assessment showed comparable γH2AX signal profiles in mock-treated, 80 mJ, and 130 mJ groups. The 180 mJ group exhibited a clear shift toward higher intensities and broader distribution, indicating increased single-cell DNA damage.

Quantification of γH2AX-positive cells

γH2AX levels (percentage of positive nuclei per field) were unaffected at 80 mJ (mean difference: −0.03747; 95% CI: −11.04 to 10.96; $p > 0.99$) and 130 mJ (mean difference: 0.4579; 95% CI: −10.54 to 11.46; $p > 0.99$) versus controls. Irradiation at 180 mJ resulted in a significant approximately twofold increase in γH2AX-positive cells (mean difference: −29.98; 95% CI: −40.98 to −18.99; $p < 0.001$).

Summary

Low- and moderate-energy irradiation did not significantly increase γH2AX. High-energy irradiation (180 mJ) produced a pronounced, threshold-dependent elevation in γH2AX signal and positive cell proportion, consistent with proliferative suppression and induction of apoptosis and necrosis (one-way ANOVA, Dunnett's test; $p < 0.001$; Figures 4 and 5).

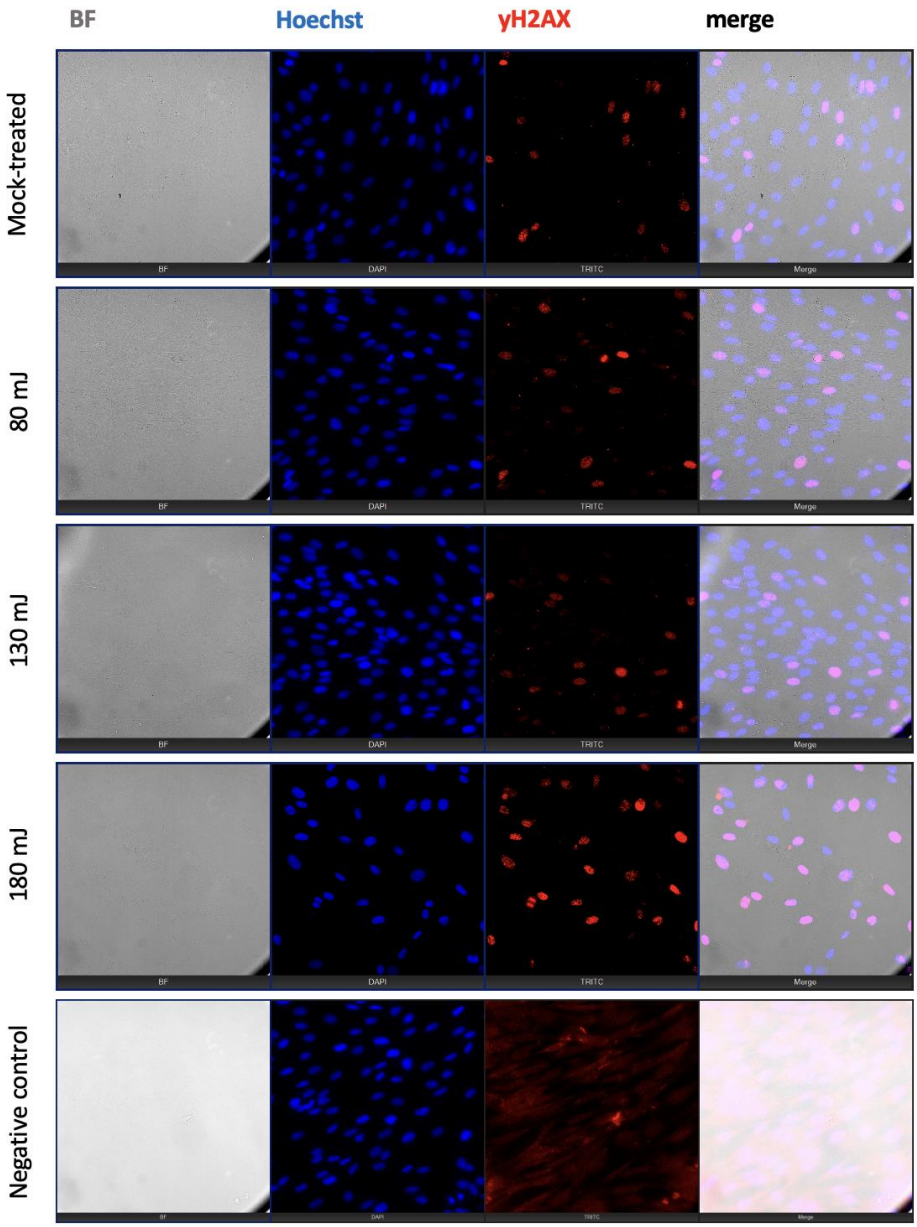

Fig. 4. Immunofluorescent detection of DNA damage signal (γH2AX) in HFF-1 fibroblasts following Er:YAG laser irradiation. Representative immunofluorescence images at 80 mJ, 130 mJ, and 180 mJ compared with mock-treated controls and negative control (primary antibody omitted). Brightfield (BF), nuclear staining (Hoechst, blue), γH2AX immunofluorescence (red), and merged images. Magnification: ×40

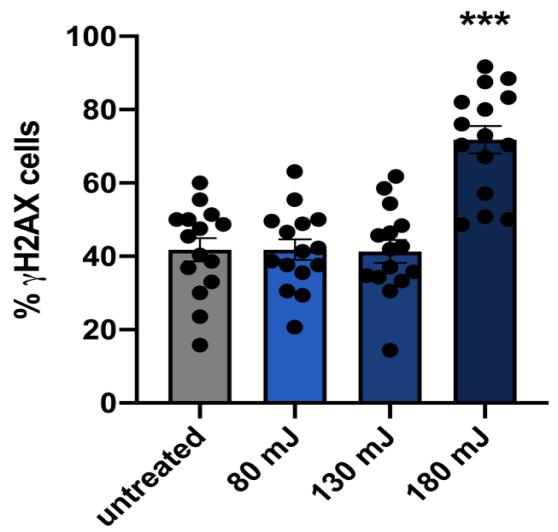

Fig. 5. Effects of Er:YAG laser irradiation on DNA damage in human fiobroblasts (γH2AX immunofluorescence). Quantification of γH2AX-positive cells (%), individual data points shown, bars representing mean ± SEM (N = 3; n = 15 per group)

DISCUSSION

This study demonstrates a dose-dependent transition in Er:YAG laser effects on human fibroblasts, with low--to-moderate irradiation (80–130 mJ) producing limited cellular perturbation and high-energy exposure (180 mJ) triggering significant DNA damage, proliferative arrest, and dual activation of apoptotic and necrotic pathways.

Dose-dependent proliferative effects

The observed proliferative suppression contrasts with reports of stimulatory effects at lower energy densities. Ogita et al. [5] demonstrated enhanced gingival fibroblast proliferation at 3.37 J/cm², and Lin et al. [1] reported that 4.2 J/cm² promoted wound healing via galectin-7 upregulation. The stimulatory effects of low--level laser therapy are mediated through cytochrome c oxidase activation, ATP production, ROS modulation, and downstream proliferative signaling [7,10]. The fluences applied in the present study (28.6–64.3 J/cm²) substantially exceed these stimulatory ranges, likely explaining the absence of proliferative enhancement and the emergence of cytotoxic responses at 180 mJ [1,5,7,10].

The absence of early-phase (2–8 h) significance may reflect genuine biological latency, as DNA damage checkpoints and downstream proliferative arrest typically require several hours to manifest at the population level; however, a contribution from the sensitivity ceiling of nuclear stain-based automated counting cannot be excluded, as the observed differences (mean < 0.15 proliferation ratio units) may fall within assay detection variability. These possibilities are not mutually exclusive and cannot be resolved from the present data.

4γH2AX-associated DNA damage signaling

Phosphorylation of H2AX at Ser139 is an early, sensitive marker of DNA double-strand breaks and a platform for DNA repair machinery recruitment [19,20,21]. The approximately twofold increase in γH2AX-positive cells at 180 mJ is consistent with Pan et al.'s [14] demonstration of dose-dependent p53 activation, vacuolization, and necrosis following Er:YAG irradiation. γH2AX phosphorylation, mediated by ataxia telangiectasia mutated (ATM), ataxia telangiectasia and Rad3-related (ATR) and DNA-dependent protein kinase (DNA-PK) activates cell cycle checkpoints that either promote repair or, when damage is irreparable, trigger apoptosis [22,23,24,25]. The sustained proliferative suppression through 24 h alongside elevated γH2AX confirms persistent checkpoint activation preventing cell cycle progression.

Apoptosis versus necrosis

Concurrent elevation of Annexin V- and EthD-III--positive cells at 180 mJ indicates dual activation of cell death pathways. Mild-to-moderate DNA damage typically activates p53-dependent apoptosis via BAX, PUMA, and NOXA upregulation [26], while severe damage leads to necrosis through energy depletion or membrane failure [27]. High-fluence irradiation generates excessive mitochondrial ROS, driving mitochondrial permeability transition and cytochrome c release [28,29,30]. Wu et al. [29] showed that high--fluence low-power laser irradiation (120 J/cm²) induced apoptosis through ROS-mediated mitochondrial permeability transition, with cyclosporine A-sensitive and BAX-dependent pathways. The coexistence of apoptotic and necrotic populations at 180 mJ suggests that the magnitude of stress exceeds ordered apoptotic capacity in a subset of cells. The absence of significant cell death at 80 and 130 mJ, despite modest late--phase proliferative suppression, defines a range of biologically tolerable irradiation [30,31,32].

Clinical implications

The biological transition identified between 130 and 180 mJ under the tested conditions aligns with clinical observations of increasing complication rates at higher ablation depths – 10.1% for superficial versus 26.5% for deeper Er:YAG resurfacing [15] and 40% transient hyperpigmentation following variable-pulsed treatment [16], suggesting these outcomes may partly reflect the cellular stress responses characterised here. While direct translation from a single-cell-line in vitro model

to clinical practice requires caution, the finding that energies ≤130 mJ preserved viability and produced no detectable DNA damage or cell death under controlled conditions provides a preliminary cellular-level rationale for favouring conservative energy parameters, particularly in applications where fibroblast preservation is therapeutically important, such as wound healing and tissue remodeling.

Stimulatory versus photothermal mechanisms

The shift from stimulatory to cytotoxic effects likely reflects a transition from photochemical to photothermal mechanisms. At low energy densities, sublethal thermal stress may activate heat shock proteins without irreversible damage [33]. At higher energies, strong water absorption at 2940 nm generates sufficient temperature elevations to denature proteins, disrupt membranes, and induce DNA strand breaks through thermal or oxidative mechanisms [13,14]. Hympanova et al. [4] documented temperature increases, extracellular matrix coagulation, and subsequent fibroblast proliferation and collagen remodeling following non-ablative Er:YAG irradiation, consistent with the integrated cellular responses observed here.

Limitations and future directions

Key limitations include the use of only three discrete energy levels, precluding precise cytotoxic threshold delineation; reliance on γH2AX immunofluorescence alone, which reflects double- strand break signaling without characterizing lesion type, repair dynamics, or distinguishing transient from persistent damage; absence of direct mechanistic assessment of ROS generation, mitochondrial dysfunction, or ATM/ATR/p53 pathway activation; potential optical confounding from residual culture medium during irradiation; and the inherent constraints of a single--cell-line in vitro model, which does not replicate multicellular tissue architecture, vascularization, or immune interactions. Future work should incorporate additional cell types, refined dose titration, complementary molecular assays, and advanced in vitro and in vivo validation.

CONCLUSIONS

This study characterizes the dose-dependent effects of Er:YAG laser irradiation on human fibroblasts across proliferation, cell death, and DNA damage endpoints. Low-to-moderate irradiation (80–130 mJ) was associated with preserved viability and undetectable DNA damage, despite measurable late-phase proliferative suppression. Irradiation at 180 mJ produced a distinct cytotoxic profile: elevated γH2AX signaling, sustained proliferative arrest, and concurrent apoptotic and necrotic cell death. These results should be interpreted as preliminary in vitro reference points rather than clinically applicable thresholds, given the model's inherent limitations. Translational validation in advanced models is required before these findings can inform clinical protocols.

Supplementary materials

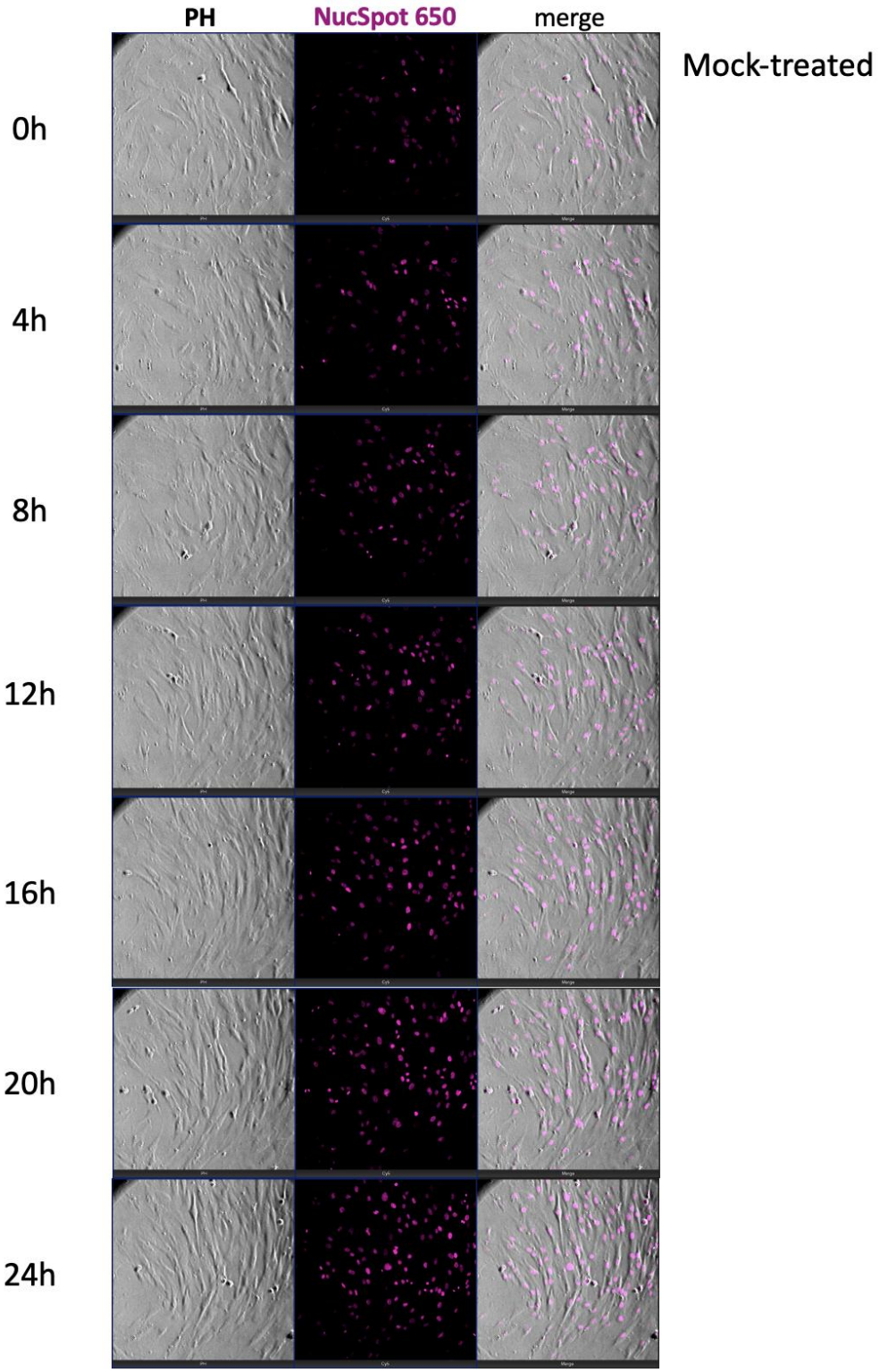

Fig. S1. Mock-treated control (proliferation time-lapse). Time-lapse imaging of mock-treated HFF-1 fibroblasts over 24 h following procedural handling without laser activation. Cells were stained with NucSpot Live 650 to enable automated nuclear detection and quantification. Phase contrast (PH), fluorescence (NucSpot 650), and merged images are shown at 0, 4, 8, 12, 16, 20, and 24 h. A progressive increase in cell number is observed over time, reflecting normal proliferative activity under baseline conditions. Nuclear morphology remains uniform, with no visible signs of cellular stress or detachment

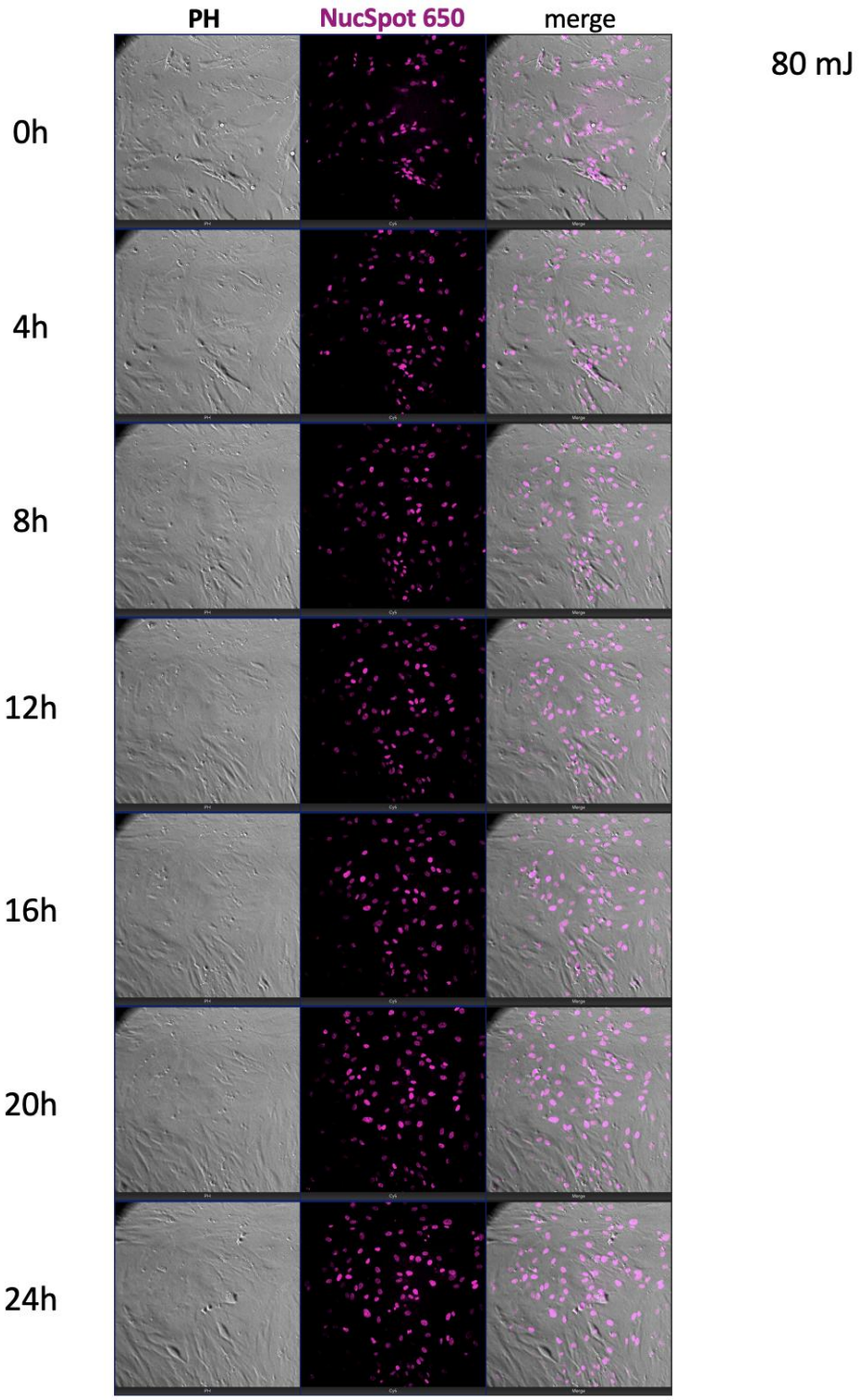

Fig. S2. 80 mJ irradiation (proliferation time-lapse). Time-lapse imaging of HFF-1 fibroblasts following Er:YAG laser irradiation at 80 mJ. Cells were stained with NucSpot Live 650 and monitored for 24 h. Phase contrast (PH), fluorescence, and merged images are presented at indicated time points. Compared with mock-treated controls, a modest attenuation of proliferation is observed at later time points, while overall cell morphology and adherence remain preserved. No overt signs of cytotoxicity are evident

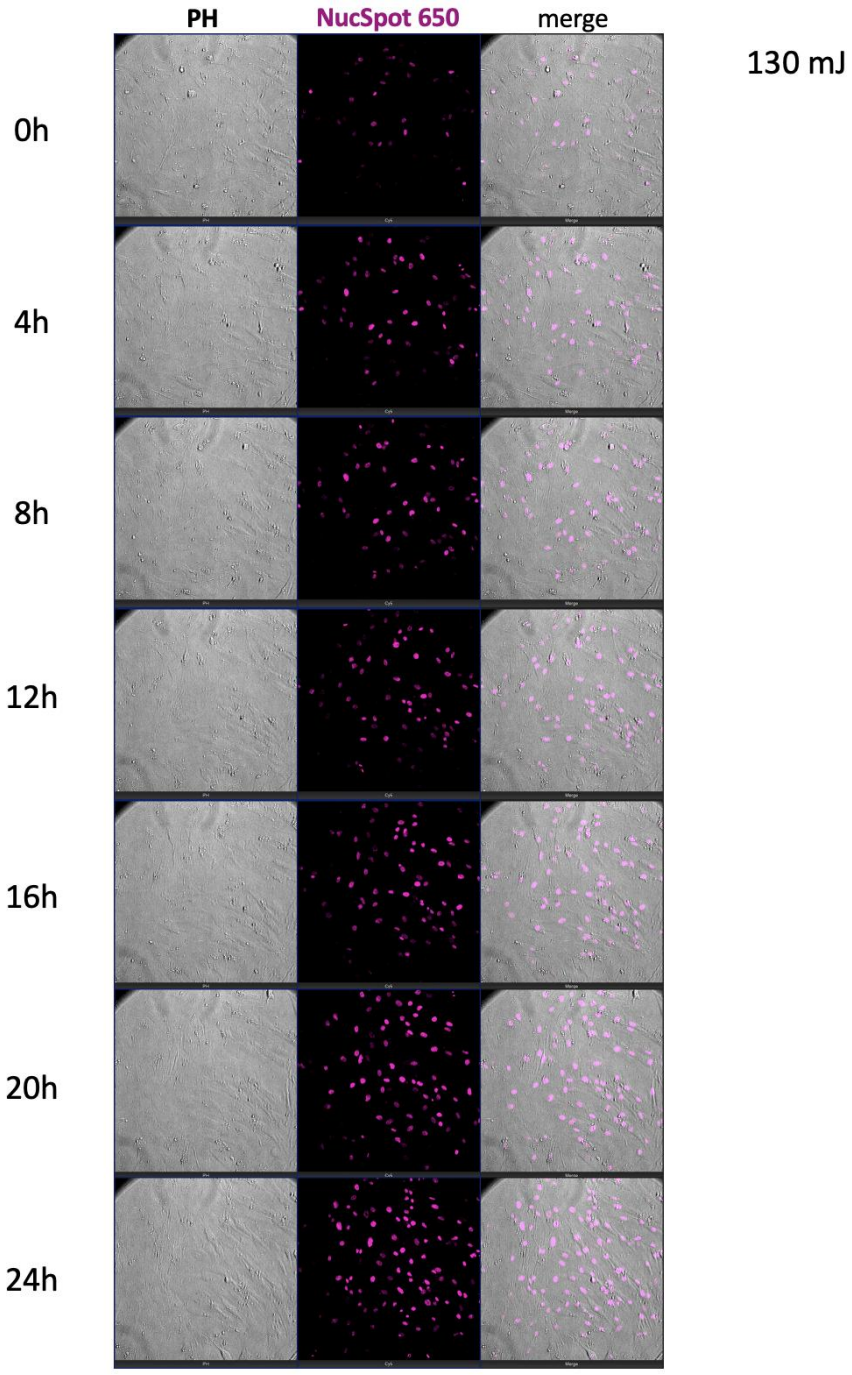

Fig. S3. 130 mJ irradiation (proliferation time-lapse). Time-lapse imaging of HFF-1 fibroblasts following Er:YAG laser irradiation at 130 mJ. Cells were stained with NucSpot Live 650 and imaged over 24 h. A reduction in cell density relative to mock-treated controls becomes more apparent over time, indicating suppressed proliferative activity. Cellular morphology remains largely intact, with preserved adherence and no clear evidence of widespread cell death within the observed time frame

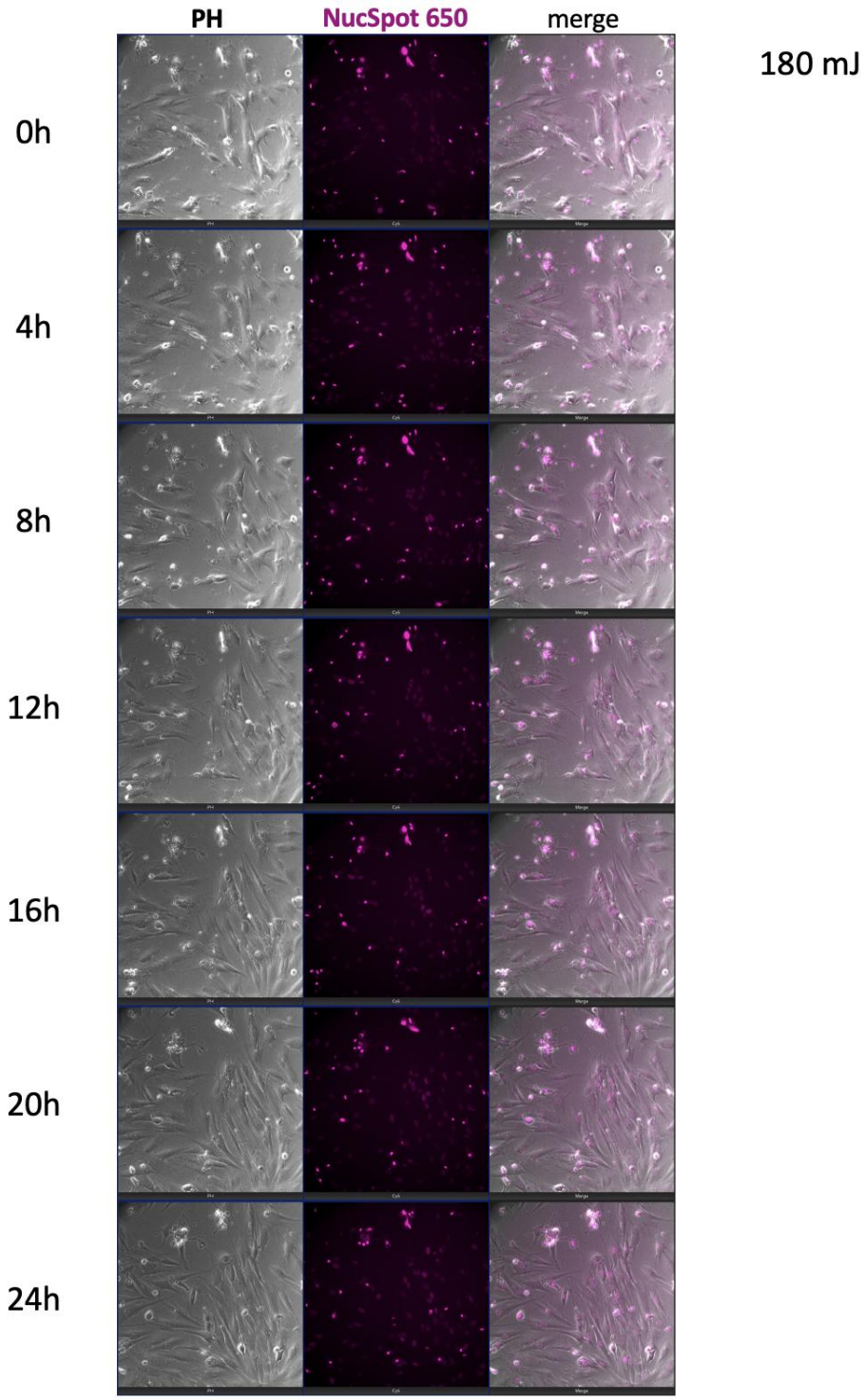

Fig. S4. 180 mJ irradiation (proliferation time-lapse). Time-lapse imaging of HFF-1 fibroblasts following Er:YAG laser irradiation at 180 mJ. Cells were stained with NucSpot Live 650 and monitored for 24 h. A marked reduction in cell number and altered cellular morphology are observed compared with lower energy conditions and mock-treated controls. Cells exhibit decreased confluence, irregular morphology, and features consistent with cellular stress and loss of viability, indicating a cytotoxic effect at this energy level

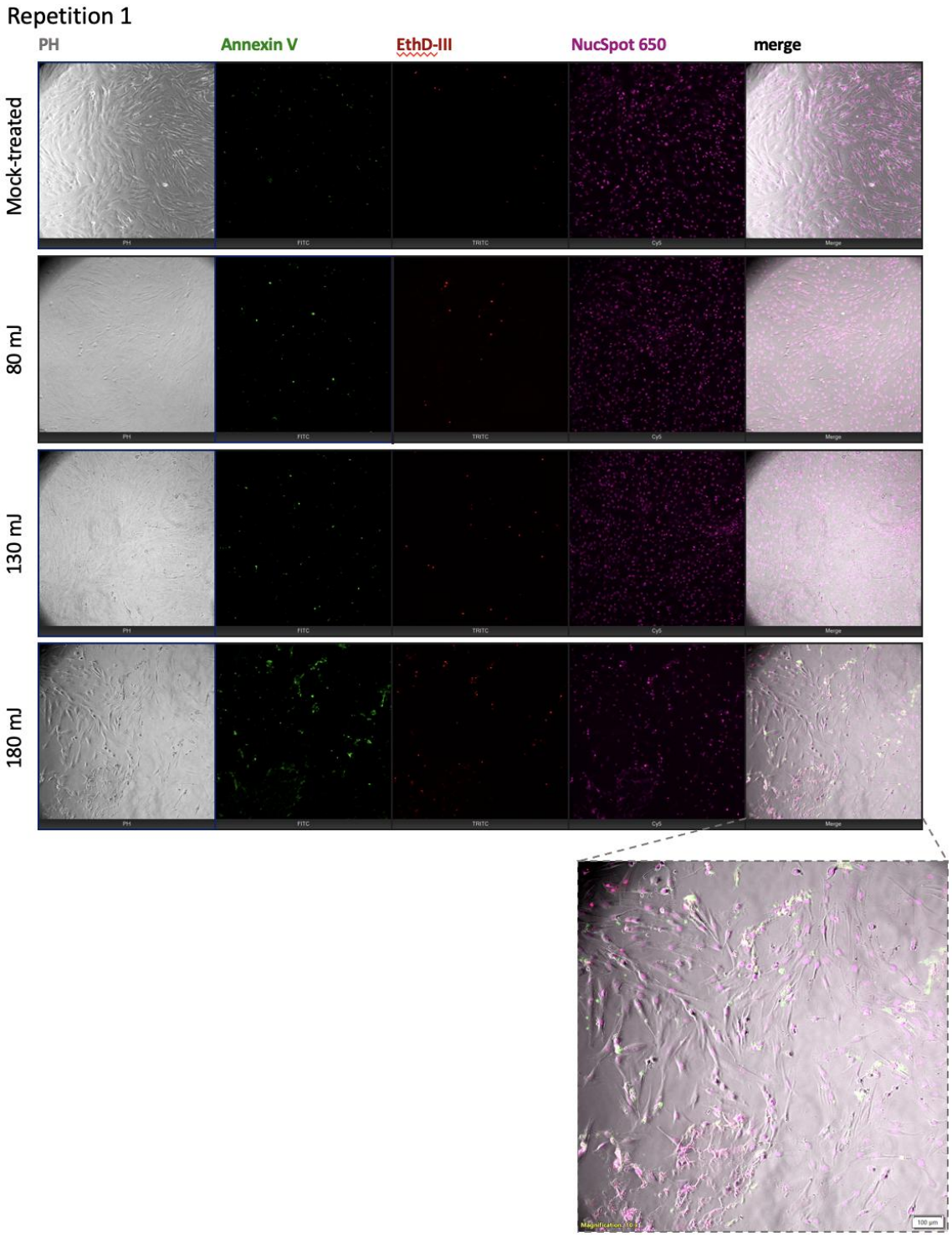

Fig. S5. Annexin V / EthD-III assay – Repetition 1. Representative fluorescence microscopy images of HFF-1 fibroblasts following Er:YAG laser irradiation at 80 mJ, 130 mJ, and 180 mJ compared with mock-treated controls. Cells were stained with Annexin V (green; early apoptosis), EthD-III (red; necrosis), and NucSpot 650 (magenta; nuclei), with corresponding phase contrast (PH) and merged images. Minimal Annexin V and EthD-III signals are observed in mock--treated and low-energy groups (80 mJ, 130 mJ). In contrast, the 180 mJ condition demonstrates increased Annexin V and EthD-III signal intensity and frequency, indicating induction of apoptotic and necrotic cell death. Insets show higher magnification of the 180 mJ condition

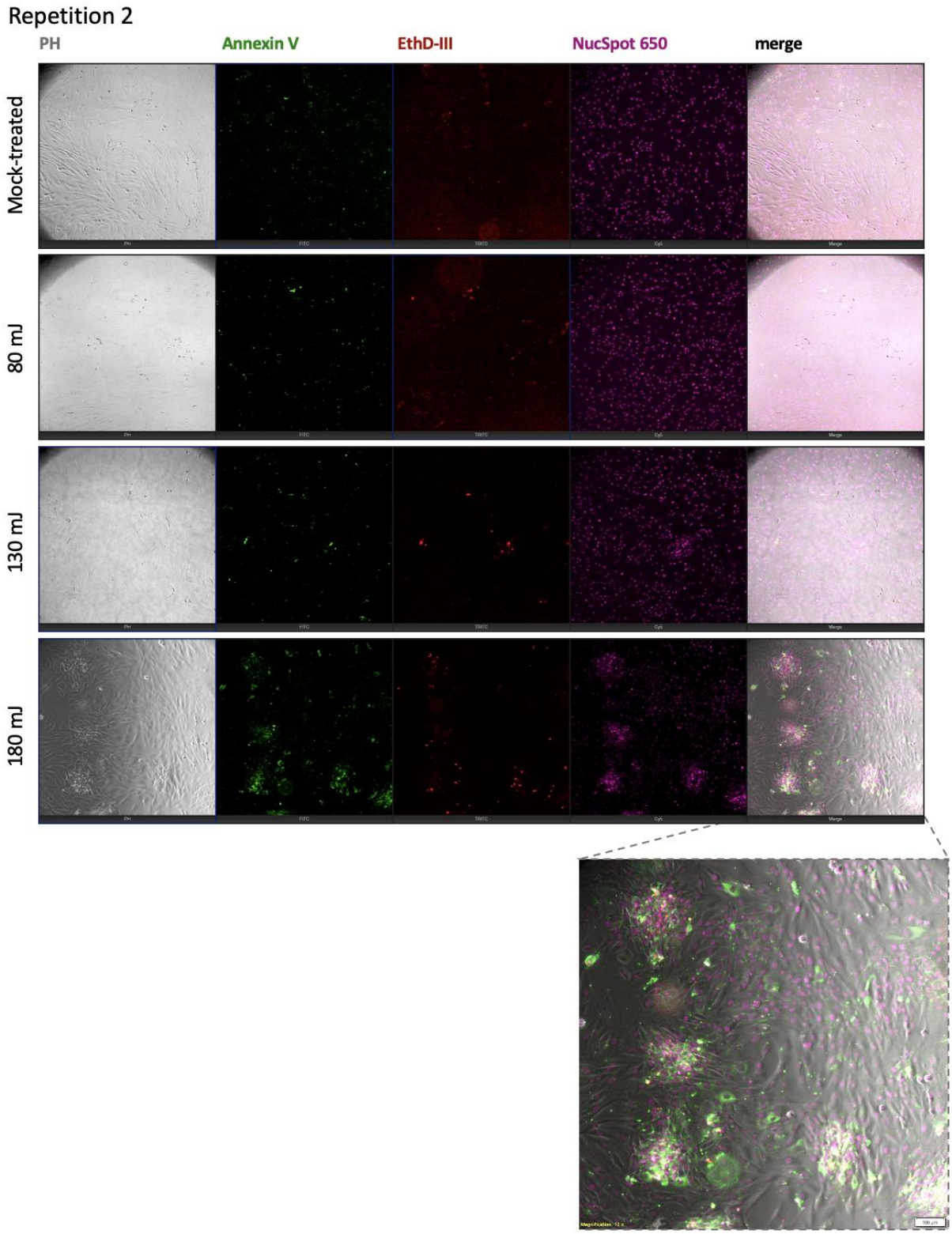

Fig. S6. Annexin V / EthD-III assay – Repetition 2. Representative images of HFF-1 fibroblasts stained with Annexin V (green), EthD-III (red), and NucSpot 650 (magenta) following Er:YAG laser irradiation. Mock-treated and lower energy groups (80 mJ, 130 mJ) exhibit low levels of apoptotic and necrotic staining. The 180 mJ condition shows a marked increase in Annexin V-positive cells and detectable EthD-III signal, accompanied by altered cell morphology and reduced confluence in phase contrast images. High-magnification inset highlights areas of increased apoptotic signal

Conflict of interest

The Authors declare no conflict of interest.

Funding statement

This research received no external funding.

Use of AI tools statement

Grammarly AI was used for language correction.

Authors' contribution

Study design – J. Fiegler-Rudol, R.D. Wojtyczka
Data collection – J. Fiegler-Rudol, R.D. Wojtyczka
Data interpretation – J. Fiegler-Rudol, J. Matys, R. Wiench
Statistical analysis – J. Fiegler-Rudol, J. Matys, R. Wiench
Manuscript preparation – J. Fiegler-Rudol, J. Matys, D.R. Skaba
Literature research – J. Fiegler-Rudol, D.R. Skaba, R. Wiench

REFERENCES

1. Lin T, Yu CC, Liu CM, Hsieh PL, Liao YW, Yu CH, et al. Er:YAG laser promotes proliferation and wound healing capacity of human periodontal ligament fibroblasts through galectin-7 induction. J Formos Med Assoc. 2021;120(1 Pt 2):388–394. doi: 10.1016/j.jfma.2020.06.005.

2. Pourzarandian A, Watanabe H, Ruwanpura SM, Aoki A, Noguchi K, Ishikawa I. Er:YAG laser irradiation increases prostaglandin E production via the induction of cyclooxygenase-2 mRNA in human gingival fibroblasts. J Periodontal Res. 2005;40(2):182–186. doi: 10.1111/j.1600-0765.2005.00789.x.

3. Pourzarandian A, Watanabe H, Ruwanpura SM, Aoki A, Ishikawa I. Effect of low-level Er:YAG laser irradiation on cultured human gingival fibroblasts. J Periodontol. 2005;76(2):187–193. doi: 10.1902/jop.2005.76.2.187.

4. Hympanova L, Mackova K, El-Domyati M, Vodegel E, Roovers JP, Bosteels J, et al. Effects of non-ablative Er:YAG laser on the skin and the vaginal wall: systematic review of the clinical and experimental literature. Int Urogynecol J. 2020;31(12):2473–2484. doi: 10.1007/s00192-020-04452-9.

5. Ogita M, Tsuchida S, Aoki A, Satoh M, Kado S, Sawabe M, et al. Increased cell proliferation and differential protein expression induced by low-level Er:YAG laser irradiation in human gingival fibroblasts: proteomic analysis. Lasers Med Sci. 2015;30(7):1855–1866. doi: 10.1007/s10103-014-1691-4.

6. Zaitsev AE, Asanov ON. Erbium:yttrium aluminium garnet (Er:YAG) laser therapy versus sharp debridement in the management of chronic ulcers of the lower extremity: A randomized controlled trial. Int Wound J. 2025;22(6):e70688. doi: 10.1111/iwj.70688.

7. Maghfour J, Ozog DM, Mineroff J, Jagdeo J, Kohli I, Lim HW. Photobiomodulation CME part I: Overview and mechanism of action. J Am Acad Dermatol. 2024;91(5):793–802. doi: 10.1016/j.jaad.2023.10.073.

8. de Freitas LF, Hamblin MR. Proposed mechanisms of photobiomodulation or low-level light therapy. IEEE J Sel Top Quantum Electron. 2016;22(3):7000417. doi: 10.1109/JSTQE.2016.2561201.

9. Guo Z, Yuan K. The application of light emitting diode (LED) in cosmetic dermatology. Photodermatol Photoimmunol Photomed. 2025;41(5):e70041. doi: 10.1111/phpp.70041.

10. Dompe C, Moncrieff L, Matys J, Grzech-Leśniak K, Kocherova I, Bryja A, et al. Photobiomodulation-Underlying Mechanism and Clinical Applications. J Clin Med. 2020;9(6):1724. doi: 10.3390/jcm9061724.

11. Glass GE. Photobiomodulation: the clinical applications of low-level light therapy. Aesthet Surg J. 2021;41(6):723–738. doi: 10.1093/asj/sjab025.

12. Wang X, Tian F, Soni SS, Gonzalez-Lima F, Liu H. Interplay between up-regulation of cytochrome-c-oxidase and hemoglobin oxygenation induced by near-infrared laser. Sci Rep. 2016;6:30540. doi: 10.1038/srep30540.

13. Modena DAO, Miranda ACG, Grecco C, Liebano RE, Cordeiro RCT, Guidi RM. Efficacy, safety, and guidelines of application of the fractional ablative laser erbium:YAG 2940 nm and non-ablative laser erbium glass in rejuvenation, skin spots, and acne in different skin phototypes: a systematic review. Lasers Med Sci. 2020;35(9):1877–1888. doi: 10.1007/s10103-020-03046-7.

14. Pan TL, Wang PW, Lee WR, Fang CL, Chen CC, Huang CM, et al. Systematic evaluations of skin damage irradiated by an erbium:YAG laser: histopathologic analysis, proteomic profiles, and cellular response. J Dermatol Sci. 2010;58(1):8–18. doi: 10.1016/j.jdermsci.2010.02.001.

15. Weniger FG, Weidman AA, Barrero Castedo CE. Full-field erbium:YAG laser resurfacing: complications and suggested safety parameters. Aesthet Surg J. 2020;40(10):NP374–NP385. doi: 10.1093/asj/sjz319.

16. Tanzi EL, Alster TS. Side effects and complications of variable-pulsed erbium:yttrium–aluminum–garnet laser skin resurfacing: extended experience with 50 patients. Plast Reconstr Surg. 2003;111(4):1524–1529. doi: 10.1097/01.PRS.0000049647.65948.50.

17. Alsaad SM, Ross EV, Smith WJ, DeRienzo DP. Analysis of depth of ablation, thermal damage, wound healing, and wound contraction with erbium:YAG laser in a Yorkshire pig model. J Drugs Dermatol. 2015;14(11):1245–1252.

18. Fiegler-Rudol J, Kępa M, Skaba D, Wiench R. Er:YAG laser energy optimization for reducing single-species microbial growth on agar surfaces in vitro. Pathogens. 2025;14(12):1287. doi: 10.3390/pathogens14121287.

19. Trakarnphornsombat W, Kimura H. Live-cell tracking of γ-H2AX kinetics reveals the distinct modes of ATM and DNA-PK in the immediate response to DNA damage. J Cell Sci. 2023;136(8):jcs260698. doi: 10.1242/jcs.260698.

20. Prabhu KS, Kuttikrishnan S, Ahmad N, Habeeba U, Mariyam Z, Suleman M, et al. H2AX: A key player in DNA damage response and a promising target for cancer therapy. Biomed Pharmacother. 2024;175:116663. doi: 10.1016/j.biopha.2024.116663.

21. Mah LJ, El-Osta A, Karagiannis TC. gammaH2AX: a sensitive molecular marker of DNA damage and repair. Leukemia. 2010; 24(4):679–686. doi: 10.1038/leu.2010.6.

22. Rahmanian N, Shokrzadeh M, Eskandani M. Recent advances in γH2AX biomarker-based genotoxicity assays: A marker of DNA damage and repair. DNA Repair. 2021;108:103243. doi: 10.1016/j.dnarep.2021.103243.

23. Kinner A, Wu W, Staudt C, Iliakis G. Gamma-H2AX in recognition and signaling of DNA double-strand breaks in the context of chromatin. Nucleic Acids Res. 2008;36(17):5678–5694. doi: 10.1093/nar/gkn550.

24. Surova O, Zhivotovsky B. Various modes of cell death induced by DNA damage. Oncogene. 2013;32(33):3789–3797. doi: 10.1038/onc.2012.556.

25. Matt S, Hofmann TG. The DNA damage-induced cell death response: a roadmap to kill cancer cells. Cell Mol Life Sci. 2016;73(15):2829–2850. doi: 10.1007/s00018-016-2130-4.

26. Borges HL, Linden R, Wang JY. DNA damage-induced cell death: lessons from the central nervous system. Cell Res. 2008;18(1):17–26. doi: 10.1038/cr.2007.110.

27. Tu HC, Ren D, Wang GX, Chen DY, Westergard TD, Kim H, et al. The p53-cathepsin axis cooperates with ROS to activate programmed necrotic death upon DNA damage. Proc Natl Acad Sci U S A. 2009;106(4):1093–1098. doi: 10.1073/pnas.0808173106.

28. Lynnyk A, Lunova M, Jirsa M, Egorova D, Kulikov A, Kubinová Š, et al. Manipulating the mitochondria activity in human hepatic cell line Huh7 by low-power laser irradiation. Biomed Opt Express. 2018;9(3):1283–1300. doi: 10.1364/BOE.9.001283.

29. Wu S, Xing D, Wang F, Chen T, Chen WR. Mechanistic study of apoptosis induced by high-fluence low-power laser irradiation using

fluorescence imaging techniques. J Biomed Opt. 2007;12(6):064015. doi: 10.1117/1.2804923.

30. Wu S, Xing D, Gao X, Chen WR. High fluence low-power laser irradiation induces mitochondrial permeability transition mediated by reactive oxygen species. J Cell Physiol. 2009;218(3):603–611. doi: 10.1002/jcp.21636.

31. Lukac M, Zorman A, Lukac N, Perhavec T, Tasic B. Characteristics of non-ablative resurfacing of soft tissues by repetitive Er:YAG laser pulse irradiation. Lasers Surg Med. 2021;53(9):1266–1278. doi: 10.1002/lsm.23402.

32. Ross EV, McKinlay JR, Sajben FP, Miller CH, Barnette DJ, Meehan KJ, et al. Use of a novel erbium laser in a Yucatan minipig: a study of residual thermal damage, ablation, and wound healing as a function of pulse duration. Lasers Surg Med. 2002;30(2):93–100. doi: 10.1002/lsm.10030.

33. Chung H, Dai T, Sharma SK, Huang YY, Carroll JD, Hamblin MR. The nuts and bolts of low-level laser (light) therapy. Ann Biomed Eng. 2012;40(2):516–533. doi: 10.1007/s10439-011-0454-7.